

# Quantum Vortex in a Vectorial Bose-Einstein Condensate

Tomoya ISOSHIMA,\* Kazushige MACHIDA and Tetsuo OHMI<sup>1</sup>

*Department of Physics, Okayama University, Okayama 700-8530,*

<sup>1</sup>*Department of Physics, Graduate School of Science, Kyoto University, Kyoto 606-8502*

(Received December 2, 2024)

Quantum vortices in the multi-component Bose-Einstein condensation (BEC) are investigated theoretically. Three kinds of the vortex configurations are found and their physical properties are discussed in details, including the density distribution and the spin texture. By using the Bogoliubov theory extended to the three component BEC, the collective modes for these vortices are evaluated. The local vortex stability for these vortices are examined in light of the existence of the negative eigenvalue, yielding a narrow magnetization window for the local intrinsic stable region where the multi-components work together to stabilize a vortex in a self-organized way.

**KEYWORDS:** Vortex, Three component Bose-Einstein condensation, Gross-Pitaevskii equation, Bogoliubov equation, Collective modes

## §1. Introduction

There have been much attention focused on Bose-Einstein condensation (BEC) realized in alkali-metal atom gases.<sup>1,2,3)</sup> In particular, since two experimental groups<sup>4,5,6,7,8)</sup> have succeeded in producing quantum vortices in a rotating trapped BEC in <sup>87</sup>Rb system, many researchers investigate various aspects of this quantized vortex in the hope to obtain the better understanding of physical nature of superfluidity in this dilute weakly interacting Bose system. Here we have a better controlled mathematical tool, namely, Bogoliubov theory to treat it, compared with superfluid <sup>4</sup>He where no established microscopic theory to treat this strongly interacting Bose condensed system is known.

In a series of our papers<sup>9,10,11,12)</sup> we have been studying the problem of the intrinsic instability of a vortex in BEC. We are the first to point out the existence of the negative eigenvalue in the Bogoliubov excitation spectrum,<sup>9)</sup> demonstrating that a quantized vortex in BEC confined by a rigid wall is intrinsically unstable and corresponding to the Rokhsar instability<sup>13)</sup> due to the spiraling-out of a vortex core in a harmonically trapped BEC. In order to arrest this instability and to stabilize it, we propose several practical devices feasible experimentally, such as sending a laser light at the core center to raise the potential which moves up the whole Bogoliubov spectrum as a result, or raising temperature and increasing the non-condensate fraction relative to the condensation which acts as an extra potential.<sup>11)</sup> A similar recovering method is proposed by Doi<sup>14)</sup> who consider the two component BEC. We also examine the external rotation effect<sup>10)</sup> on the vortex stability and determine

the several characteristic critical rotation frequencies,<sup>12)</sup> including the lowest critical frequency which signals the first entry of a vortex upon increasing the forced rotation. This particular value<sup>12)</sup> is by far nearer to the observed stirring frequency in the recent vortex creation experiment by optical spoon<sup>6,7,8)</sup> than that estimated by the conventional Thomas-Fermi approximation. This coincidence further encourages us to perform the present study along this line.

So far in all the theories and experiments mentioned above the internal degrees of freedom in an atom is frozen by the external magnetic field serving as a confining potential. By means of optical confinement, all the hyperfine states with  $F=1$  in <sup>23</sup>Na active and three components with  $m_F = 1, 0, -1$  are simultaneously Bose-condensed,<sup>15)</sup> giving rise to a new state of matter; a BEC characterized by a vectorial order parameter. Ohmi and Machida,<sup>16)</sup> and Ho<sup>17)</sup> independently introduce the basic Hamiltonian for describing this vector BEC by extending the Bogoliubov framework and study the fundamental properties of this interesting vector BEC, pointing out the richness of the topological defect structures such as the  $l$ -vector textures, domain wall structure, etc. These are very analogous to the <sup>3</sup>He superfluid A and B phases.<sup>18)</sup> Again as the basic interaction in these superfluid Fermions is strong, we have to resort to the strong coupling theory to describe it. The existing theories for superfluid <sup>3</sup>He is quite phenomenological and difficult to derive microscopically. In contrast, our theory here is quite microscopic and there is no room to introduce phenomenological parameters in it.

Guided by this analogy, we are going to study here the vortex structures in more details. Yip<sup>19)</sup> gave the first study on a vortex in the vectorial BEC, classifying the possible vortex structures as functions of the inter-

\* E-mail: tomoya@mp.okayama-u.ac.jp

action strength of the spin channel and the magnetization of the system. Unfortunately, some of the vortices introduced by Yip (I and IV phase in ref.<sup>19)</sup>) are simply not allowed because the fundamental phase requirement is violated for these particular vortices (See eq. (8)). Leonhardt and Volovik<sup>20)</sup> propose the half-quantum vortex (Alice string). Stoof<sup>21)</sup> and Marzlin *et al*<sup>22)</sup> examine independently the skyrmion creation in the vectorial BEC. Thus, here continuing our study on the vectorial BEC,<sup>16, 23, 24, 25, 26)</sup> we perform microscopic calculations of the possible vortices in harmonically trapped vector BEC and examine the intrinsic stability problem in connection with our intrinsic instability of a vortex in the scalar BEC.

After giving the Gross-Pitaevskii equation for the vectorial BEC with the three component order parameters in next Section, we examine the fundamental phase requirements for the order parameter components when they form a vortex. We enumerate several possible vortices in a cylindrical symmetric case in §3. In §4 each of these possible vortices is studied in details: their physical properties such as the density distributions of the three components and spin configuration around a vortex core. Evaluating the excitation spectrum for each vortex form by solving the Bogoliubov equation extended to the three components, we examine the stability condition of each vortex as a function of the total magnetization in §5. The last Section is devoted to summary and discussions.

## §2. Gross-Pitaevskii Equation for Three Components

We treat a system of the Bose condensates with the internal degrees of freedom  $F = 1$  so that the order parameter is characterized by the spins:  $m_F = 1, 0, -1$ . We start with a general Hamiltonian which fully considers system's symmetries, such as translation and rotation symmetries in real space and spin space:

$$H = \int d\mathbf{r} \left[ \sum_i \Psi_i^\dagger \{h(\mathbf{r}) - \mu_i\} \Psi_i + \frac{g_n}{2} \sum_{ij} \Psi_i^\dagger \Psi_j^\dagger \Psi_j \Psi_i + \frac{g_s}{2} \sum_{\alpha} \sum_{ijkl} \Psi_i^\dagger \Psi_j^\dagger (F_\alpha)_{ik} (F_\alpha)_{jl} \Psi_k \Psi_l \right], \quad (1)$$

where

$$h(\mathbf{r}) = -\frac{\hbar^2 \nabla^2}{2m} + V(\mathbf{r}), \quad (2)$$

$$g_n = \frac{4\pi\hbar^2}{m} \cdot \frac{a_0 + 2a_2}{3}, \quad (3)$$

$$g_s = \frac{4\pi\hbar^2}{m} \cdot \frac{a_2 - a_0}{3}. \quad (4)$$

The subscripts are  $\alpha = (x, y, z)$  and  $i, j, k, l = (0, \pm 1)$  corresponding to the above three species. The chemical potentials for the three components;  $\mu_i$  ( $i = 0, \pm 1$ ) sat-

isfy  $\mu_1 + \mu_{-1} = 2\mu_0$ . The scalar field  $V(\mathbf{r})$  is the external confinement potential such as an optical potential.

Following our previous paper,<sup>16)</sup> and the usual procedure for a BEC system without spin, the Gross-Pitaevskii equation extended to the three component order parameters is obtained as

$$\left[ \left\{ h(\mathbf{r}) - \mu_i + g_n \sum_k |\phi_k|^2 \right\} \delta_{ij} + g_s \sum_{\alpha} \sum_{kl} \{ (F_\alpha)_{ij} (F_\alpha)_{kl} \phi_k^* \phi_l \} \right] \phi_j = 0. \quad (5)$$

These coupled equations for the  $j$ -th condensate  $\phi_j$  ( $j = 0, \pm 1$ ) are used to calculate various properties of a vortex in the following.

## §3. Phase Requirements of Condensates

The system is assumed to be symmetric cylindrically and the cylindrical coordinate system  $\mathbf{r} = (r, \theta, z)$  is used. The wavefunctions are divided into the radial part  $\phi$  and phase part  $\gamma$  as

$$\phi_j(r, \theta) = \phi_j(r) \gamma_j(\theta), \quad (6)$$

$$\gamma_j(\theta) = \exp[i(\alpha_j + \beta_j \theta)] \quad (7)$$

where  $j = 0, \pm 1$ . The wavefunctions  $\phi_j(r)$  are real. Temporarily we assume  $\phi_j(r) \geq 0$ . The relative phases between  $\gamma_1, \gamma_0$  and  $\gamma_{-1}$  must satisfy the condition:

$$\pm \gamma_0^2 = \gamma_{-1} \gamma_1 \quad (8)$$

which comes from the spin interaction term  $g_s$  of Hamiltonian eq. (1). This condition is rewritten in terms of  $\alpha$  and  $\beta$  as

$$2\alpha_0 = \alpha_1 + \alpha_{-1} + n\pi \quad (9)$$

$$2\beta_0 = \beta_1 + \beta_{-1} \quad (10)$$

where  $n$  is an integer. We take  $\alpha_0 = 0$  in the following. Thus the phase factors of the wavefunctions are generally written as

$$\begin{pmatrix} \gamma_1 \\ \gamma_0 \\ \gamma_{-1} \end{pmatrix} = \begin{pmatrix} \exp[i(\alpha + \beta\theta)] \\ 1 \\ \pm \exp[-i(\alpha + \beta\theta)] \end{pmatrix} \exp[i\beta_0\theta] \quad (11)$$

with

$$\beta = \beta_1 - \beta_0 = \beta_0 - \beta_{-1} \quad (12)$$

and

$$\alpha = \alpha_1 = -\alpha_{-1}. \quad (13)$$

In the followings we exclude the vortex states with winding number  $\beta_i$  larger than 1 simply because the smaller winding number, the more stable. The possible combinations for  $\beta_i$  are  $(\beta_1, \beta_0, \beta_{-1}) = (1, 0, -1), (1, 1, 1)$  and  $(1, \text{none}, 0)$ . We call the vortex state with  $(1, \text{none}, 0)$  the Alice state. The Alice string discussed by Leonhardt and Volovik<sup>20)</sup> has this combination of the winding num-

bers for the three components, although the Alice string has another condition for the amplitudes. The trivial combinations which are equivalent to the above ones, i.e.  $(-1, 0, 1), (-1, -1, -1), (-1, \text{none}, 0)$  and  $(0, \text{none}, \pm 1)$  are excluded.

The sign of  $\gamma_{-1}$  in eq. (11) is determined by the sign of  $g_s$ . See appendix of ref. 23. When  $g_s < 0$  (ferromagnetic case),  $\gamma_{-1} = +\exp[-i(\alpha + \beta\theta)]$ . When  $g_s > 0$  (antiferromagnetic case),  $\gamma_{-1} = -\exp[-i(\alpha + \beta\theta)]$ . We redefine  $\phi_{-1}$  and  $\gamma_{-1}$  for simplicity of our calculation:

$$\begin{cases} \phi_{-1}(r) \geq 0 & (\text{ferromagnetic case}) \\ \phi_{-1}(r) \leq 0 & (\text{antiferromagnetic case}) \end{cases} \quad (14)$$

$$\gamma_{-1} = \exp[-i(\alpha + \beta\theta)] \quad (15)$$

The Gross-Pitaevskii equation eq. (5) for the real wavefunctions  $\phi_j(r)$  becomes

$$\begin{aligned} & \left[ \frac{-\hbar^2}{2m} \left\{ \frac{d^2}{dr^2} + \frac{1}{r} \frac{d}{dr} - \frac{(\beta_0 + j\beta)^2}{r^2} \right\} \delta_{ij} \right. \\ & \quad \left. - \mu_i \delta_{ij} + g_n \sum_k \phi_k^2 \delta_{ij} \right. \\ & \quad \left. + g_s \sum_{\alpha} \left\{ (F_{\alpha})_{ij} \sum_{kl} (F_{\alpha})_{kl} \phi_k(r) \phi_l(r) \right\} \right] \phi_j(r) = 0. \end{aligned} \quad (16)$$

The phase  $\alpha$  does not appear here. This means that  $\phi_j(r)$  are independent of  $\alpha$ .

The total energy of the system is given by

$$\begin{aligned} E = & \int d^3\mathbf{r} \left[ \sum_j \phi_j(r) \frac{-\hbar^2}{2m} \left\{ \frac{d^2}{dr^2} + \frac{1}{r} \frac{d}{dr} - \frac{(\beta_0 + j\beta)^2}{r^2} \right\} \phi_j(r) \right. \\ & \quad \left. + \sum_j \left\{ V(r) + \frac{g_n}{2} \sum_k \phi_k^2(r) - (\mu_j - \mu_0) \right\} \phi_j^2(r) \right. \\ & \quad \left. + \frac{g_s}{2} \sum_{\alpha} \left\{ \sum_{jk} \phi_j^*(F_{\alpha})_{jk} \phi_k \right\}^2 \right]. \end{aligned} \quad (17)$$

We have done the extensive calculations to solve the above equations. The actual numerical computations are performed under the conditions: The mass and the scattering length of atoms are  $m = 3.81 \times 10^{-26} \text{ kg}$  and  $a_0 = 2.75 \text{ nm}$ . The area density of particle is  $2 \times 10^4 (\mu\text{m})^{-1}$ . These are appropriate for those of Na atom. The other scattering length  $a_2$  is defined so that  $g_s$  becomes  $\pm 0.1 g_n$ . To concentrate on a long straight vortex, we assume that the system is uniform along the  $z$  axis. Since in the ferromagnetic case the phase separation occurs, the results for a pancake shape here may be appropriate to this case. The trapping frequency is  $\omega/(2\pi) = 200 \text{ Hz}$ . The energy is scaled by the trap unit  $\hbar\omega$ . The confining potential is given by  $V(\mathbf{r}) = \frac{1}{2}m\omega^2 r^2$ . We calculate a set of the physical quantities under given parameters such as  $g_s$ , the relative polarization  $M/N$  which is determined by adjusting the chemical potentials, and the combination

of winding number  $\beta$ 's. Both ferromagnetic ( $g_s < 0$ ) and antiferromagnetic ( $g_s > 0$ ) cases are comparatively studied in the following.

#### §4. Three Kinds of Vortices

We calculate the three kinds of the vortex states for various magnetizations. The number of atoms and the magnetization are given by  $N = \sum_{i=1,0,-1} N_i$  and  $M = \sum_{i=1,0,-1} i N_i$  where  $N_i = \int |\phi_i(\mathbf{r})|^2 d\mathbf{r}$  are the number of atoms in the spin state  $i$ . The range of the relative polarization is  $-1 \leq M/N \leq 1$ . As for the  $(1, 0, -1)$  and  $(1, 1, 1)$  configurations, it is sufficient to consider the range  $0 \leq M/N \leq 1$ .

It is convenient to describe the condensates in terms of the three wavefunctions  $\phi_{\alpha}$  ( $\alpha = x, y, z$ ) where the spin quantization axis is taken along the  $\alpha$  direction:

$$\begin{pmatrix} \phi_x \\ \phi_y \\ \phi_z \end{pmatrix} = \begin{pmatrix} \frac{-1}{\sqrt{2}} & 0 & \frac{1}{\sqrt{2}} \\ \frac{-i}{\sqrt{2}} & 0 & \frac{-i}{\sqrt{2}} \\ \frac{1}{\sqrt{2}} & 1 & 0 \end{pmatrix} \begin{pmatrix} \phi_1 \\ \phi_0 \\ \phi_{-1} \end{pmatrix}. \quad (18)$$

Let define the  $m$ - and  $n$ -vectors as

$$\mathbf{m} = (m_x, m_y, m_z) = \text{Re}(\phi_x, \phi_y, \phi_z) \quad (19)$$

$$\mathbf{n} = (n_x, n_y, n_z) = \text{Im}(\phi_x, \phi_y, \phi_z). \quad (20)$$

where  $\mathbf{m}$  and  $\mathbf{n}$  are real vectors. The  $l$ -vector which points the direction of the local magnetization is  $\mathbf{l} = \mathbf{m} \times \mathbf{n}$ . The corresponding unit vector is  $\hat{\mathbf{l}}$ .

##### 4.1 Alice states

When the phase configuration of the condensates is the Alice type:

$$\begin{pmatrix} \phi_1 \\ \phi_0 \\ \phi_{-1} \end{pmatrix} = \begin{pmatrix} \phi_1(r)e^{i\theta} \\ 0 \\ \phi_{-1}(r) \end{pmatrix}, \quad (21)$$

the  $l$ -vector is always parallel to the  $z$ -axis:  $l_x = l_y = 0$ ,  $l_z = \phi_1^2 - \phi_{-1}^2$ . The zero component of the condensate  $\phi_0$  is always zero and the system is the 2-component, consisting of  $\phi_1$  and  $\phi_{-1}$ .

When the interaction is ferromagnetic, it is conceivable that one of the two components vanishes and the condensate reduces to the single component system. However, when the +1 component carries the phase winding, the other component may appear at the center of the vortex. In fact, as shown in Fig. 1(a) where density profiles of the Alice state are displayed, the core region of the +1 component is filled by the remaining component -1.

When the interaction is antiferromagnetic, the amplitude ratio of the two components may vary continuously, depending on the magnetization. Figure 1(b) shows the case when  $M/N = 0.531$ . For all ranges of  $M/N$ , the density of the +1 component has a peak at  $r \simeq 3 \mu\text{m}$ .

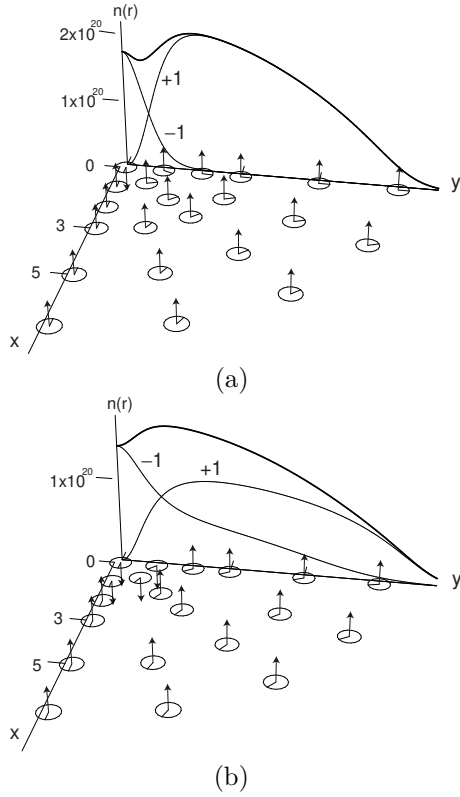


Fig. 1. The density profiles of the condensates are displayed along the radial direction and the  $\hat{l}$ -vector in the Alice type vortex is shown for the quadrant in the  $(x, y)$  plane. The vertical axis is the density of the condensates. The upper bold curve shows the total density  $n(r)$  and the thin curves show the density of each component  $n_i(r)$ . The arrows on the  $(x, y)$  plane are the  $\hat{l}$ -vectors. The small circles are perpendicular to each  $\hat{l}$ -vector and the short rods show  $m$ -vectors. They are depicted at  $r = \sqrt{x^2 + y^2} = 0, 1, 2, 3, 5$ , and  $7 \mu\text{m}$ . (a) Ferromagnetic case. The magnetization  $M/N = 0.967$ . (b) Antiferromagnetic case.  $M/N = 0.531$ . Note that the intermediate magnetization like this is not possible for the ferromagnetic case.

#### 4.2 $(1, 0, -1)$ vortex

In this vortex, the condensate is described by

$$\begin{pmatrix} \phi_1 \\ \phi_0 \\ \phi_{-1} \end{pmatrix} = \begin{pmatrix} \phi_1(r)e^{i(\beta\theta+\alpha)} \\ \phi_0(r) \\ \phi_{-1}(r)e^{-i(\beta\theta+\alpha)} \end{pmatrix}. \quad (22)$$

The winding number of  $\phi_0$  is zero and the 0 component is only the component of the condensates which can exist at the vortex center. The magnetization of the condensate can vary continuously in this configuration of the winding number. The  $l$ -vector is given by

$$\begin{pmatrix} l_x \\ l_y \end{pmatrix} = \phi_0(r) \frac{\phi_1(r) + \phi_{-1}(r)}{\sqrt{2}} \begin{pmatrix} \cos(\alpha + \beta\theta) \\ -\sin(\alpha + \beta\theta) \end{pmatrix} \quad (23)$$

$$l_z = \frac{\phi_1^2(r) - \phi_{-1}^2(r)}{2} \quad (24)$$

Figure 2 shows the  $l_x$  and  $l_y$  configurations in the  $(x, y)$  plane for the two kinds of the disgyration with either

$\beta = 1$  or  $\beta = -1$ .

Figures 3(a) and (b) show the particle density profiles along the radial direction in the ferromagnetic case. It is seen from Fig. 3(a) that the  $\phi_0$  component fills in the core region, thus there is no appreciable particle number depleted region near the center. Notice that  $\phi_{-1}(r) \leq 0$  when the interaction is ferromagnetic.

The corresponding antiferromagnetic case for the  $(1, 0, -1)$  vortex is displayed in Fig. 4(a) and (b). Here it is also true that the large number of the  $\phi_0$  component occupies the core region, pushing out  $\phi_1$  and  $\phi_{-1}$ . The total particle number almost smoothly decreases outwardly.

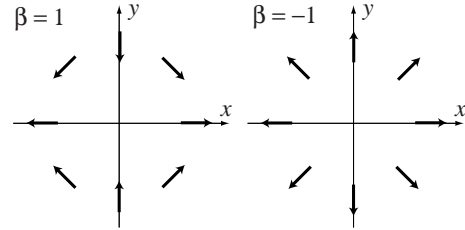


Fig. 2. The bold arrows show  $x$  and  $y$  component of  $l$ -vectors when winding number combination is  $(1, 0, -1)$  for the ferromagnetic case ( $\alpha = 0$ ). The  $l$ -vectors show cross disgyration when  $\beta = 1$  and radial disgyration when  $\beta = -1$ . For the antiferromagnetic case the direction of the  $l$ -vectors in the  $(x, y)$  plane is reversed.

#### 4.3 $(1, 1, 1)$ vortex

All of components have the winding number 1 in this vortex, namely, the wavefunction is written in the form:

$$\begin{pmatrix} \phi_1 \\ \phi_0 \\ \phi_{-1} \end{pmatrix} = \begin{pmatrix} \phi_1(r) \\ \phi_0(r) \\ \phi_{-1}(r) \end{pmatrix} e^{i\theta} \quad (25)$$

It is shown that the  $l$ -vector does not depend on  $\theta$ .

$$\mathbf{l} = \begin{pmatrix} \phi_0 \frac{\phi_1 + \phi_{-1}}{\sqrt{2}} \cos(\alpha) \\ \phi_0 \frac{\phi_1 + \phi_{-1}}{\sqrt{2}} \sin(-\alpha) \\ \frac{1}{2}(\phi_1^2 - \phi_{-1}^2) \end{pmatrix}. \quad (26)$$

For the ferromagnetic case, this reduces to single component BEC. Figure 5 shows the typical results for this case, namely, as all the components have non-vanishing phase winding, the densities vanish at the vortex core center. The total density distribution looks like a vortex in the scalar BEC. For the antiferromagnetic case, the  $l$ -vector given by eq. (26) vanishes when  $|\phi_{-1}| = |\phi_1|$ .

## §5. Local Stability of Vortex State

### 5.1 Formulation

In order to determine the intrinsic stability condition for each vortex state without the external rotation, we

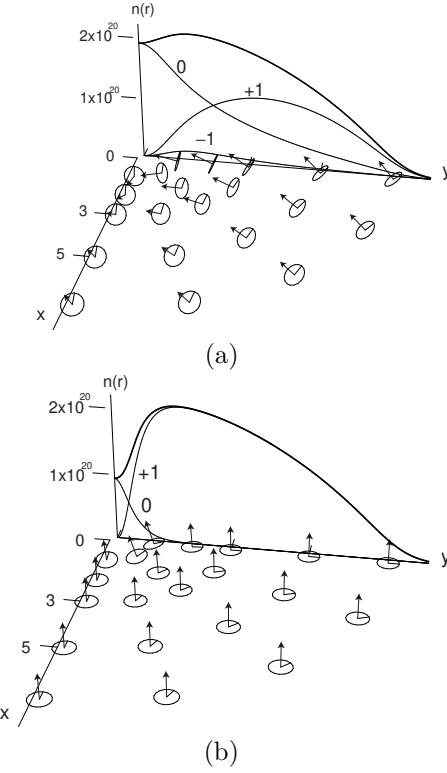


Fig. 3. The density profiles of the condensates and the  $\hat{l}$ -vector when the interaction is ferromagnetic and the winding number combination is  $(1, 0, -1)$ . The vertical axis is the density of the condensate. The upper bold curve shows the total density  $n(r)$  and the thin curves show the density of each component  $n_i(r)$ . (a)  $M/N = 0.612$ . (b)  $M/N = 0.994$ .

give the formulation for evaluating the excitation spectrum of the three component BEC, which is based on the Bogoliubov theory extended to take into account the spin degrees of freedom. The collective excitation spectrum of the condensate, whose static properties are determined by the Gross-Pitaevskii equation eq. (5), is a solution of the Bogoliubov equations given by

$$\sum_j \{A_{ij}u_q(\mathbf{r}, j) - B_{ij}v_q(\mathbf{r}, j)\} = \varepsilon_q u_q(\mathbf{r}, i), \quad (27)$$

$$\sum_j \{B_{ij}^*u_q(\mathbf{r}, j) - A_{ij}^*v_q(\mathbf{r}, j)\} = \varepsilon_q v_q(\mathbf{r}, i) \quad (28)$$

where

$$\begin{aligned} A_{ij} &= h(\mathbf{r})\delta_{ij} - \mu_i\delta_{ij} \\ &+ g_n \left\{ \sum_k |\phi_k|^2 \delta_{ij} + \phi_i \phi_j^* \right\} \\ &+ g_s \sum_{\alpha} \sum_{kl} [(F_{\alpha})_{ij} (F_{\alpha})_{kl} \phi_k^* \phi_l \\ &+ (F_{\alpha})_{il} (F_{\alpha})_{kj} (\phi_k^* \phi_l)], \end{aligned} \quad (29)$$

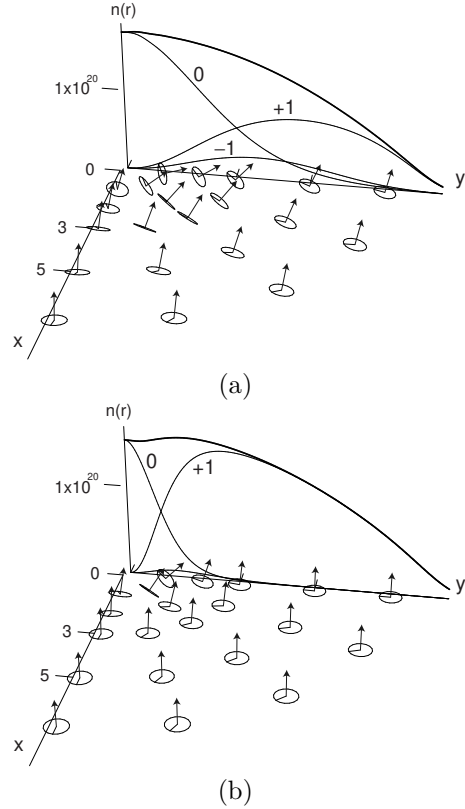


Fig. 4. The density profiles of the condensates and the  $\hat{l}$ -vector when the interaction is antiferromagnetic and the winding number combination is  $(1, 0, -1)$ . The vertical axis is the density of the condensate. The upper bold curve shows the total density  $n(r)$  and the thin curves show the density of each component  $n_i(r)$ . (a)  $M/N = 0.474$ . (b)  $M/N = 0.952$ .

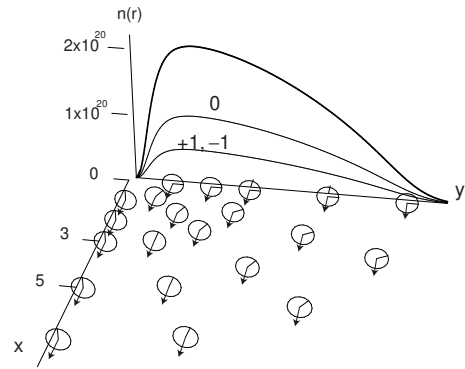


Fig. 5. The density profile of the condensate and the  $\hat{l}$ -vector for the ferromagnetic case of the  $(1, 1, 1)$  vortex. The magnetization  $M/N = 0$ . The vertical axis is the density of the condensate. The upper bold curve shows the total density  $n(r)$  and the thin curves show the density of each component  $n_i(r)$ .

$$B_{ij} = g_n \phi_i \phi_j + g_s \sum_{\alpha} \sum_{kl} [(F_{\alpha})_{ik} \phi_k (F_{\alpha})_{jl} \phi_l], \quad (30)$$

$u_q(\mathbf{r}, i)$  and  $v_q(\mathbf{r}, i)$  are the  $q$ -th eigenfunctions with the spin  $i$  and  $\varepsilon_q$  corresponds to the  $q$ -th eigenvalue.

We are treating a cylindrical system  $\mathbf{r} = (r, \theta, z)$ . The relevant physical quantities are written in the following form up to the phase factor:

$$u_q(\mathbf{r}, j) = u_q(r, j) e^{i(q\theta + \beta_0)\theta} e^{i(\alpha + \beta\theta)j}, \quad (31)$$

$$v_q(\mathbf{r}, j) = v_q(r, j) e^{i(q\theta - \beta_0)\theta} e^{-i(\alpha + \beta\theta)j}, \quad (32)$$

with the angular momentum  $q\theta$ . (The momentum  $q_z$  along the  $z$  direction is ignored.)

### 5.2 Stable range

When all of the excitation levels have the positive eigenvalue, the vortex state is stable,<sup>9, 10)</sup> namely, the vortex is locally stable in the energy configuration space. Thus the stable region of the magnetization for a given vortex is determined by evaluating the whole excitation spectrum of the above Bogoliubov equations: eqs. (27) and (28). We calculate them to check if there exists the negative eigenvalue. This procedure yields the stable magnetization region. It should be noted that the lowest level at the particular angular momentum  $q\theta = -1$  in the excitation spectrum often becomes negative, signaling the local instability of a vortex as discussed in the single component BEC.<sup>9, 12)</sup> The positive spectrum does not mean that this vortex is stable globally relative to other states, such as non-vortex state. Let us discuss here the local stability of our enumerated vortices. The stable ranges for the magnetization where the negative mode does not appear and system is stable for each vortex are listed below:

(1) For the (1,0,-1) vortex configuration in the ferromagnetic case, the stable range of  $M/N$  is determined as

$$0.992 < M/N < 0.999 \quad (\text{ferromagnetic (1,0,-1) vortex}) \quad (33)$$

The typical density profile and excitation spectrum are shown in Figs. 6(a) and (b) where the left hand side column depicts the density distributions for each component and the right hand side column shows the corresponding excitation spectrum as a function of the angular momentum  $q\theta$ . The magnetization is  $M/N = 0.998$  here.

(2) For the (1,0,-1) vortex in the antiferromagnetic case, the stable range is given by

$$0.988 < M/N < 0.999 \quad (\text{antiferromagnetic (1,0,-1) vortex}) \quad (34)$$

We show the density profile and the excitation spectrum in Figs. 6(c) and (d). The magnetization is  $M/N = 0.994$  here. Comparing the above ferromagnetic case, because the magnetization decrease the 0-component fills in more the vortex core region. It pushes up the lowest excitation

and stabilizes this vortex as a result.

(3) In the Alice vortex of the antiferromagnetic case, the stable range is determined as

$$0.972 < M/N < 0.999 \quad (\text{antiferromagnetic Alice vortex}) \quad (35)$$

We display the density profile and the excitation spectrum for this stable Alice vortex in Figs. 6(e) and (f). The density distribution of the antiferromagnetic Alice vortex is very similar to that in the (1,0,-1) vortex shown in Fig. 6 (a) and (c).

It is rather remarkable that these multiple components work together so as to stabilize the vortex locally. As the magnetization decreases from  $M/N = 1$ , the lowest eigenvalue at  $q\theta = -1$  becomes positive. Upon further decreasing beyond the critical magnetization, its eigenvalue becomes negative again, indicating the local instability. This was not seen in the single component case where the vortex is always locally unstable.<sup>9, 12)</sup> This becomes stable only when the system is subjected under external rotation or when introducing the pinning potential.

It is generally seen throughout these vortices that the component with the winding number 0 fills in the core region of the +1 component with the winding 1. This 0-winding component stabilize the vortex state. For the two component BEC, a similar stabilization mechanism is considered by Doi.<sup>14)</sup>

The locally stable regions are limited to the cases where the magnetizations are close to the full polarized state. If the magnetization increases further towards the complete polarization, the system effectively becomes one component BEC and shows the local instability which was studied previously in details.<sup>9, 12)</sup>

## §6. Summary and Conclusion

We have established a general framework to calculate various physical properties of a vortex in a cylindrical symmetric situation for a three component BEC system with  $m_F = 1, 0, -1$  of  $F = 1$ . This allows us to evaluate the density distributions of the multiple component BEC, and the spatial variations of the triad  $(m, n, l)$  which fully characterize a vortex. This theoretical framework yields not only the above static properties, but also the dynamical properties, such as the collective modes. The latter is used to examine the local stability of a vortex.

In the present paper, we have taken up three typical vortices which might be realized in the actual experimental situations, namely, the phase windings of the wave functions for the three components  $\phi_1, \phi_0$  and  $\phi_{-1}$  are given by (1,0,-1), (1,1,1) and (1, none, 0) as the representative vortices.

We have characterized these vortices for both ferromagnetic and antiferromagnetic interaction cases. In general, the 0-winding component, if any, fills in the core

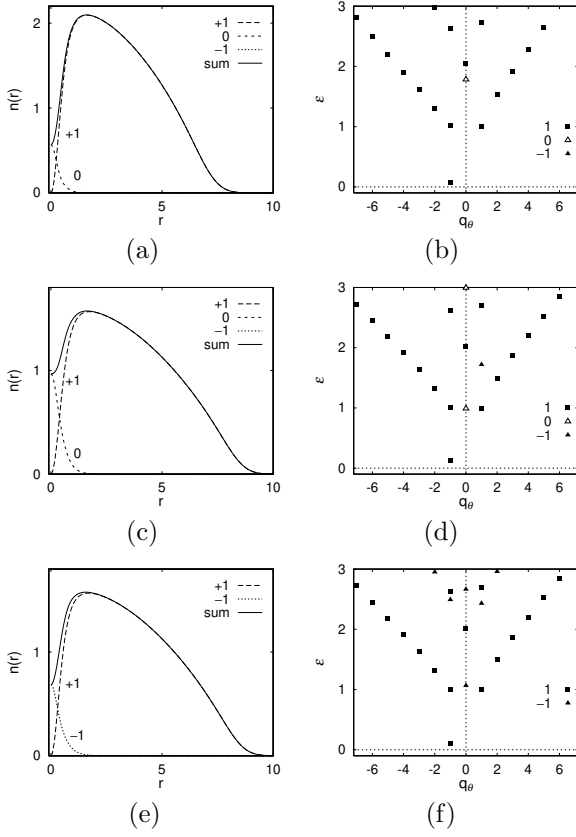


Fig. 6. The density profiles (in the units of  $10^{20} \text{m}^{-3}$  and  $\mu\text{m}$ ); (a), (c) and (e), and the corresponding excitation spectra; (b), (d) and (f) for the locally stable vortices. The eigenvalues are normalized by  $\hbar\omega$  and characterized by different marks, indicating where the eigenvalues belong. (a) and (b) Ferromagnetic  $(1,0,-1)$  vortex,  $M/N = 0.998$ . (c) and (d) Antiferromagnetic  $(1,0,-1)$  vortex,  $M/N = 0.994$ . (e) and (f) Antiferromagnetic Alice vortex,  $M/N = 0.991$ .

region. The densities of each component vary smoothly in the harmonically trapped confinement potential along the radial direction. The triad  $(\mathbf{m}, \mathbf{n}, \mathbf{l})$  yields a particular texture for each vortex. Especially, the  $l$ -vector which is proportional to the magnetization gives rise to a texture pattern, which should be observed by various experimental techniques.

The Bogoliubov equations: eqs. (27) and (28) which yield the collective excitations have been extended to the three components. We calculate the excitations for the above three kinds of the vortices and examine the stability condition as a function of the magnetization which can be controlled experimentally. Contrary to the single component BEC, the multi-component BEC allows a narrow intrinsic stability region for the magnetization, where the multiple components work to stabilize the vortex to raise the otherwise negative eigenvalue at  $q_\theta = -1$  to a positive value, that is, the non-winding component fills in the core region, effectively serving as a pinning potential. This self-organization in the multiple com-

ponent systems for the intrinsic vortex stabilization is rather remarkable, because in the single component BEC the vortex is never stabilized without the external forced rotation.<sup>9, 12)</sup> We naively expect that under the forced rotation these vortices enumerated here are easier to stabilize compare to the single BEC vortex. We will study it near future.

- [1] M. H. Anderson, J. R. Ensher, M. R. Matthews, C. E. Wieman and E. A. Cornell: *Science* **269** (1995) 198.
- [2] C. C. Bradley, C. A. Sackett, J. J. Tollett and R. G. Hulet: *Phys. Rev. Lett.* **75** (1995) 1687.
- [3] K. B. Davis, M.-O. Mewes, M. R. Andrews, N. J. van Druten, D. D. Durfee, D. M. Kurn and W. Ketterle: *Phys. Rev. Lett.* **75** (1995) 3969.
- [4] M. R. Matthews, B. P. Anderson, P. C. Haljan, D. S. Hall, C. E. Wieman and E. A. Cornell: *Phys. Rev. Lett.* **83** (1999) 2498.
- [5] B.P. Anderson, P.C. Haljan, C.E. Wieman and E.A.Cornell: *Phys. Rev. Lett.* **85** (2000) 2857.
- [6] K.W. Madison, F. Chevy, W. Wohlleben and J. Dalibard: *Phys. Rev. Lett.* **84** (2000) 806.
- [7] K.W. Madison, F. Chevy, W. Wohlleben and J. Dalibard: *cond-mat/0004037*.
- [8] F. Chevy, K.W. Madison and J. Dalibard: *Phys. Rev. Lett.* **85** (2000) 2223.
- [9] T. Isoshima and K. Machida: *J. Phys. Soc. Jpn.* **66** (1997) 3502.
- [10] T. Isoshima and K. Machida: *J. Phys. Soc. Jpn.* **68** (1999) 487.
- [11] T. Isoshima and K. Machida: *Phys. Rev. A* **59** (1999) 2203.
- [12] T. Isoshima and K. Machida: *Phys. Rev. A* **60** (1999) 3313.
- [13] D.S. Rokhsar: *Phys. Rev. Lett.* **79** (1997) 2164. D. A. Butts and D. S. Rokhsar: *Nature* **397** (1999) 327.
- [14] K. Doi and Y. Natsume: *J. Phys. Soc. Jpn.* (2001) **70** in press.
- [15] J. Stenger, S. Inouye, D. M. Stamper-Kurn, H.-J. Miesner, A. P. Chikkatur and W. Ketterle: *Nature* **369** (1998) 345. H.-J. Miesner, D. M. Stamper-Kurn, J. Stenger, S. Inouye, A. P. Chikkatur and W. Ketterle: *Phys. Rev. Lett.* **82** (1999) 2228. D. M. Stamper-Kurn, H.-J. Miesner, A. P. Chikkatur, S. Inouye, J. Stenger and W. Ketterle: *Phys. Rev. Lett.* **83** (1999) 661.
- [16] T. Ohmi and K. Machida: *J. Phys. Soc. Jpn.* **67** (1998) 1822.
- [17] T.-L. Ho: *Phys. Rev. Lett.* **81** (1998) 742.
- [18] D. Vollhardt and P. Wölfle: *The Superfluid Phases of He 3* (Taylor-Francis, London, 1990)
- [19] S.-K. Yip: *Phys. Rev. Lett.* **83** (1999) 4677.
- [20] U. Leonhardt and G. E. Volovik: *JETP Lett.* **72** (2000) 46.
- [21] H.T.C. Stoof: *cond-mat/0002375*.
- [22] Karl-Peter Marzlin, Weiping Zhang and Barry C. Sanders: *Phys. Rev. A* **62** (2000) 013602
- [23] T. Isoshima, K. Machida and T. Ohmi: *Phys. Rev. A* **60** (1999) 4857.
- [24] T. Isoshima, M. Nakahara, T. Ohmi and K. Machida: *Phys. Rev. A* **61** (2000) 063610.
- [25] M. Nakahara, T. Isoshima, K. Machida, S. Ogawa and T. Ohmi: *Physica B* **284-288** (2000) 17.
- [26] T. Isoshima, T. Ohmi and K. Machida: *J. Phys. Soc. Jpn.* **69** (2000) No.12.